On the Effects of Mobility Uncertainties on Wireless Communications Between Flying Drones in the mmWave/THz Bands

Zhangyu Guan and Tejas Kulkarni
Department of Electrical Engineering
State University of New York (SUNY) at Buffalo, NY 14260, USA
E-mail: {guan, tejaskul}@buffalo.edu

***Abstract*—Millimeter wave and terahertz (mmWave/THz) band communications are a promising technology to alleviate the looming spectrum crunch crisis in traditional RF spectrum bands. This article investigates the challenges in enabling mmWave/THz-band communications for wireless drone networking. To reduce the negative effects of high atmospheric absorption and path loss in radio in-air communications in the mmWave/THz bands, directional transmissions have been widely adopted. However, the directional mmWave/THz links with narrow beamwidth can be easily degraded or disconnected because of the misalignment between the transmit and receive antennas of the communicating drones.**

To address this challenge, in this article we take an initial step towards understanding the effects of mobility uncertainties on mmWave/THz-band communications between flying drones. We first conduct a series of field experiments to measure the mobility uncertainties of flying drones in micro, small and large scales. Then, the capacity of the mmWave/THz links achievable in the presence of mobility uncertainties is analyzed. Results indicate that micro-scale mobility has only negligible effects on the link capacity (less than 1%), while the wireless links may experience significant capacity degradation (over 50%) in the presence of small- and large-scale mobility.

***Index Terms*—Millimeter Wave/Terahertz Bands, Wireless Drone Networking, Directional Communications.**

I. Introduction

Millimeter wave and terahertz (mmWave/THz) band communications are promising technologies to alleviate the looming spectrum crunch crisis in traditional microwave wireless systems [1]–[3]. In this article we focus on investigating the challenges towards enabling high-data-rate low-latency infrastructure-less wireless drone networking with mmWave/THz-band communications.

With the wide spectrum bandwidth in 30 GHz – 100 GHz up to 0.1 THz – 10 THz, mmWave/THz-band communications have been envisioned as key technologies to support multimedia-rich applications in next-generation wireless networks with data rate from multi-Gbps to Tbps, e.g., Ultra High Definition (UHD) video, uncompressed UHD video, and wireless virtual/augmented reality [4], among others. However, the radio in-air communications in very high frequency range suffers from significant atmospheric absorption and path loss. To overcome this challenge, directional transmissions have been widely adopted for mmWave/THz communications, e.g., by forming *pencil-like* beams (i.e., beams with very narrow beamwidth) with massive antenna arrays [1], [5]. As a result, when it goes to mobile scenarios (e.g., wireless drone networking as in this article), the directional mmWave/THz links with narrow beamwidth can be easily degraded or disconnected because of the misalignment between the transmit and receive antennas. To enable mobile wireless networking in the mmWave/THz bands, it is vital to study the effects of mobility uncertainties on directional communications.

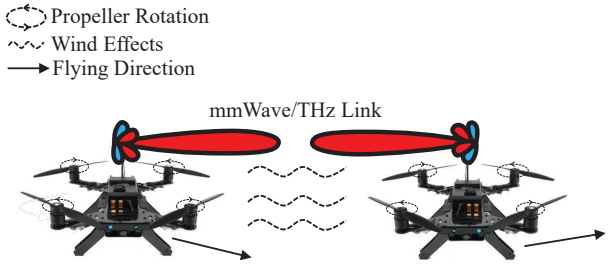

Fig. 1: Wireless communications between flying drones in the mmWave/THz bands with mobility uncertainties.

As illustrated in Fig. 1, in this work we study the effects of mobility uncertainties on mmWave/THz-band communications between flying drones. A wide set of new applications can be envisioned by enabling aerial wireless networking in the mmWave/THz bands, e.g., wireless backhauling for cellular networks with mobile hotspots [6]–[8], distributed beamforming with collaborative drones [9], high-throughput and secure tactical wireless networking in contested environments [10], and distributed aerial edge computing [11], among others. The main contributions of this work are as follows:

- **Field Measurements**. We first conduct a series of field experiments to measure the mobility uncertainties of flying drones in micro, small as well as large scales. The micro-scale mobility measures the effects of propeller rotation and engine operation of the drones, while the small- and large-scale mobility captures the mobility behaviors of the drones when they are hovering and in movement, respectively.
- **Capacity Analysis**. The link capacity achievable in the presence of multi-scale mobility uncertainties is analyzed

based on simulations. We find that the link capacity degradation caused by propeller rotation and engine operation (i.e., micro-scale mobility) is less than 1% and hence the corresponding impacts can be neglected in the protocol design for wireless drone networking in the mmWave/THz bands. When the drones are hovering or flying, the degradation can be up to 50% compared to the optimal link capacity, which therefore requires further investigation to design adaptive transmission schemes.

To the best of our knowledge, this is the first work that studies mmWave/THz-band wireless communications between flying drones.

II. Related Work

Directional mmWave/THz band communications have been studied in existing literature focusing on WLANs in mmWave bands [12], [13], vehicular networking in THz bands [14], [15], as well as THz mobile heterogeneous networks [3], [16]. For example, in [12] Haider et al. designed a mobility resilient protocol for directional 60 GHz WLANs with joint rate and beamwidth adaptation. The impact of interference from the side lanes on mmWave/THz band V2V communications with directional antennas is studied in [15]. Readers are referred to [2], [17], [18] and references therein for an excellent survey of the main results in this area. None of these existing work has explicitly considered the impacts of small-scale mobility uncertainties on mmWave/THz-band communications. The work closest to ours is [19], in which Petrov et al. studied the effects of small-scale mobility on terahertz communications focusing on indoor applications, including gaming, flight simulator and video watching. Differently, in this work we focus on outdoor wireless networking of flying drones, where both the transmitter and receiver are mobile. Finally, in [20] Kovalchukov et al. analyzed the effects of directionality and random heights on drone-based mmWave communications, but without considering the small-scale mobility of the drones.

III. Background of mmWave/THz Communications

We consider wireless communications between flying drones in the mmWave/THz bands, as illustrated in Fig. 1. Let P_{tra} and P_{rcv} represent the power of the transmitted and received signal, respectively. Denote f_0 as the central frequency and B as the bandwidth of the signal. Then the received power P_{rcv} can be given as [21]

$$P_{rcv} = A_{rcv} g(l) \int_{f_0-B/2}^{f_0+B/2} W_{tra}(f) |H_{chn}(f,l)|^2 |H_{rcv}(f,l)|^2 df, \quad (1)$$

where $W_{tra}(f)$ is the single-sided power spectral density (p.s.d) of the transmitted signal at frequency $f \in [f_0 - \frac{B}{2} \;\; f_0 + \frac{B}{2}]$, with $P_{tra} = \int_{f_0-B/2}^{f_0+B/2} W_{tra}(f) df$; $g(l)$ represents the spreading attenuation coefficient with l being the propagation distance; $H_{chn}(f,l)$ is the THz-band frequency response of the wireless channel, while $H_{rcv}(f,l)$ denotes the frequency response of the receiver and is considered an ideal low-pass filter with bandwidth B; and finally A_{rcv} is the effective receiving area, which depends on the size of the receive antenna and the relative locations and orientations of the transmit and receive antennas.

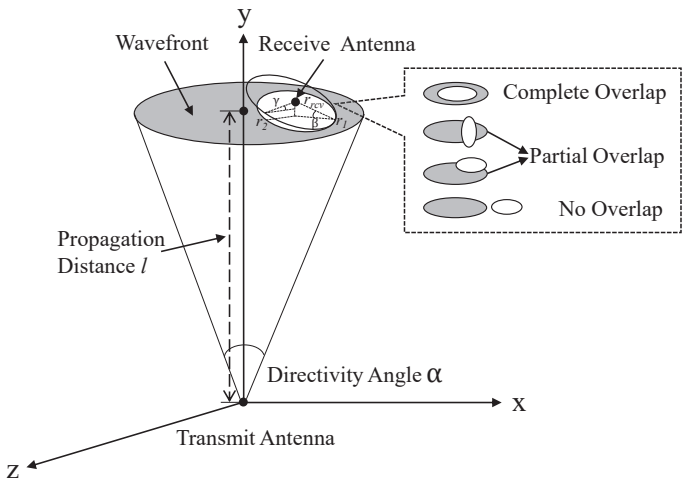

Fig. 2: Cone antenna model for mmWave/THz signal propagation in the presence of misalignment between transmit and receive antennas.

The in-air propagation of mmWave/THz signals suffers from both spreading attenuation and molecular absorption loss [1]. As illustrated in Fig. 2, we consider a cone antenna model for the spreading attenuation, while this work can be easily extended to other antenna models, e.g., the cone-plus-sphere antenna model [22]. Then, according to the free-space propagation loss (FSPL) formula, the spreading attenuation coefficient $g(l)$ in (1) can be expressed as

$$g(l) = \frac{1}{A_{frt}(l)}, \quad (2)$$

where

$$A_{frt}(l) = 2\pi l^2 (1 - \cos(\alpha/2)) \quad (3)$$

represents the area of the wavefront of the signal after propagating distance l, with α being the directivity angle of the transmit antenna [22]. Further denote $k_{abs}(f)$ as the molecular absorption coefficient for mmWave/THz signals of frequency f. Then, the overall channel frequency response $H_{chn}(f,l)$ in (1), which accounts for both the spreading and absorption attenuation, can be represented as

$$H_{chn}(f,l) = \frac{c_{lgt}}{4\pi f l} e^{-\frac{k_{abs}(f) l}{2}}, \quad (4)$$

with c_{lgt} being the speed of light.

IV. Mobility Uncertainties

As discussed in Section III, the power of the received mmWave/THz signals depends on the effective receiving area, i.e., A_{rcv} in (1), which further depends on the time-varying relative locations of the drones as well as the rotation and inclination angles of the transmit and receive antennas. Next, we first conduct a series of field experiments to measure the mobility uncertainties of the flying drones.

Field Measurements of Drone Mobility. As shown in Fig. 3, an Intel Aero Ready-to-Fly (RtF) drone is used in

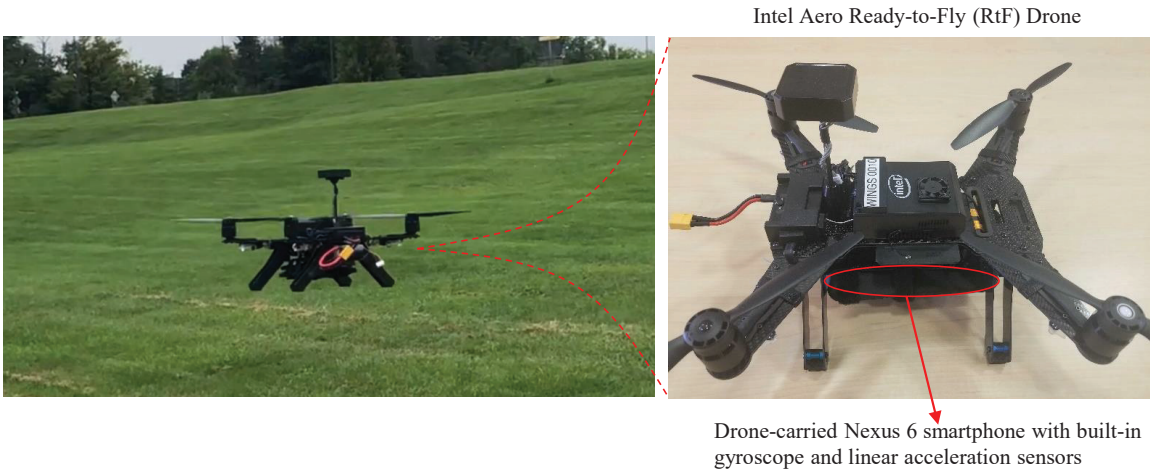

Fig. 3: Field measurement of the mobility behavior of flying drones.

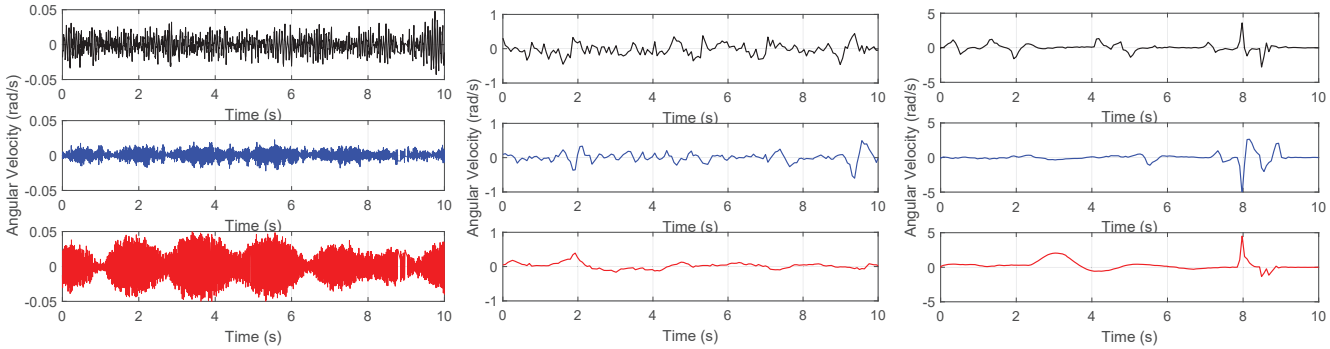

Fig. 4: Measurement results of the drone mobility with (a) micro-, (b) small-, and (c) large-scale uncertainties.

the experiments. The drone carries a Nexus 6 smartphone with built-in gyroscope and linear acceleration sensors. The gyroscope sensor is used to measure the angular velocity of the orientation and rotation of the drone, and the linear acceleration sensor measures the acceleration of the drone movement excluding the effect of the gravity of Earth. The sensed information is recorded by the Sensor Kinetics App running in the smartphone for further analysis.

Three scenarios are considered in the experiments to capture the mobility uncertainties of the drone in micro, small and large scales, caused by the engine operation and propeller rotation of the drone, the disturbance when hovering in windy environments, and the in-flight instability, respectively. The sampling rate is configured to 200 Hz for the gyroscope and linear acceleration sensors. Each instance of the measurements lasts 10 seconds. Examples of the gyroscope measurement results are reported in Fig. 4. In each figure, the top, middle and bottom subfigures plot the roll, pitch and yaw angular velocity (in $\mathrm{rad/s}$) of the drone, respectively. From Fig. 4(a) it can be seen that, in the presence of only micro-scale mobility the drone experiences very frequent fluctuations but in a small range. Differently, the fluctuations resulting from small- and large-scale mobility are less frequent but in larger ranges, as shown in Figs. 4(b) and (c).

Effective Receiving Area. With the measured information, the relative location, orientation and inclination of the transmit and receive drones can then be calculated, including the relative roll and pitch angles (i.e., β and γ in Fig. 2) and hence the effective receiving area A_{rcv} in (1).

At a specific time instant t, as illustrated in Fig. 2, the surface of the receive antenna may completely or partially overlap, or does not overlap with the wavefront. For the sake of convenient representation, consider in Fig. 2 that the transmit antenna is located at the origin and the wavefront is perpendicular to the x-z plane. Then the effective receiving area, i.e., the projection of the receive antenna surface onto the x-z plane, is an ellipse with radius

$$r_1 = r_{rcv} \cos\beta, \tag{5}$$

$$r_2 = r_{rcv} \cos\gamma, \tag{6}$$

with r_{rcv} being the radius of the receive antenna, β and γ representing the roll and pitch angles of the receive antenna with respect to x- and z-axis, respectively, as illustrated in Fig. 2. The effective receiving area can then be expressed as, taking the case of complete overlap as an example,

$$\begin{aligned} A_{rcv} &= \pi r_1 r_2 \\ &= \pi r_{rcv}^2 \cos\beta \cos\gamma. \end{aligned} \tag{7}$$

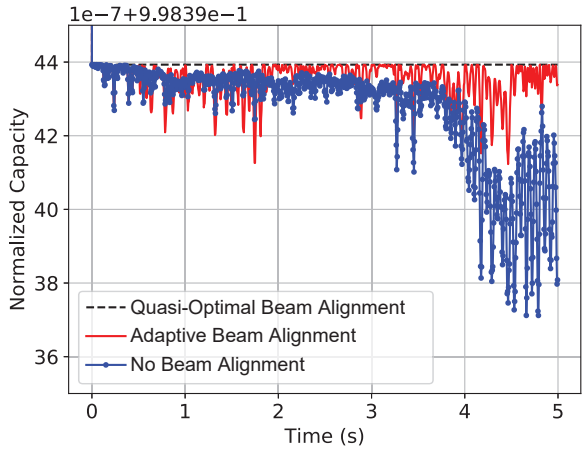

Fig. 5: Normalized link capacity with micro-scale mobility and directivity angle of 10°.

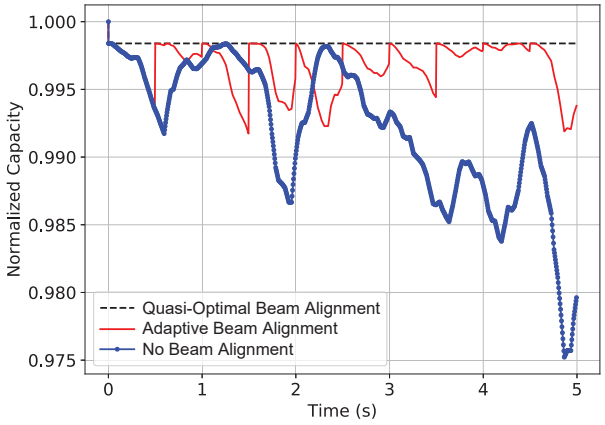

Fig. 6: Normalized link capacity with small-scale mobility and directivity angle of 10°.

Finally, the reception SNR, denoted as SNR_{rcv}, can be written as

$$SNR_{rcv} = \frac{P_{rcv}}{N_{rcv}}, \tag{8}$$

where the power of the received signal P_{rcv} is defined in (1), N_{rcv} is the molecular absorption noise power at a transmission distance l and can be expressed as [23]

$$N_{rcv} = \int_{f_0-\frac{B}{2}}^{f_0+\frac{B}{2}} (W_{back}(f) + W_{self})|H_{rcv}|^2 df. \tag{9}$$

with W_{back} and W_{self} being the background atmospheric noise p.s.d and the self-induced noise p.s.d, respectively. The link capacity C can then be calculated as

$$C = B\log_2(1 + SNR_{rcv}) \tag{10}$$

with B being the bandwidth of the transmitted signals.

V. The Effects of Mobility

To study the effects of the mobility uncertainties measured in Section IV on mmWave/THz wireless links, four scenarios are considered. In Scenarios 1, 2 and 4, the transmitter and receiver drones experience micro-, small- and large-scale mobility, respectively. In Scenario 3, the transmitter drone is subject to micro-scale mobility while the receiver drone is subject to small-scale mobility. Frequency band of $275-325$ GHz is considered, and the directivity angle is set to 5° and 10°. Three beam alignment schemes are investigated: i) quasi-optimal beam alignment, which assumes single sampling interval for the beam alignment latency, i.e., 5ms in this work; ii) adaptive beam alignment, where the beam alignment latency is set to 100 sampling intervals, i.e., 0.5s; and iii) no beam alignment. The link capacity achievable by each of the three schemes is normalized with respect to the optimal link capacity, i.e., the capacity with perfect alignment between the transmit and receive antennas. The code to repeat experiments is available on website: https://github.com/ubwingslab/Spectrum-Coexistence-FlyingTera.

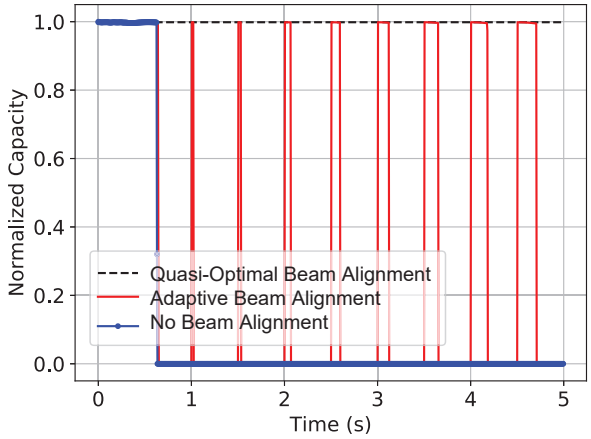

Fig. 7: Normalized link capacity with large-scale mobility and directivity angle of 10°.

Figure 5 reports the results of Scenario 1 with directivity angle of 10°. It can be found that, while the link capacity achievable in the presence of micro-scale mobility experiences very frequent fluctuations, the performance degradation compared to the optimal link capacity is negligible only (less than 1%). This means that the negative effects of micro-scale mobility can be safely neglected in the design of communication protocols for wireless drone networking in the mmWave/THz bands.

The results in Scenario 2 is reported in Fig. 6 with directivity angle of 10°. It can be seen that there is a noticeable performance degradation in the presence of small-scale mobility, which is around 2.5% after 5 seconds without beam alignment. Since the performance degradation may increase with time, certain adaptations are required to recover from the misalignment in this scenario. For example, in the case of quasi-optimal beam alignment, i.e., the alignment latency is 5ms, there are no noticeable fluctuations in the normalized capacity. If the beam alignment latency is 0.5s (i.e., adaptive beam alignment in Fig. 6), the capacity degradation can be effectively reduced to less than 1%. In this scenario the link capacity degradation is dominated by fluctuations much less

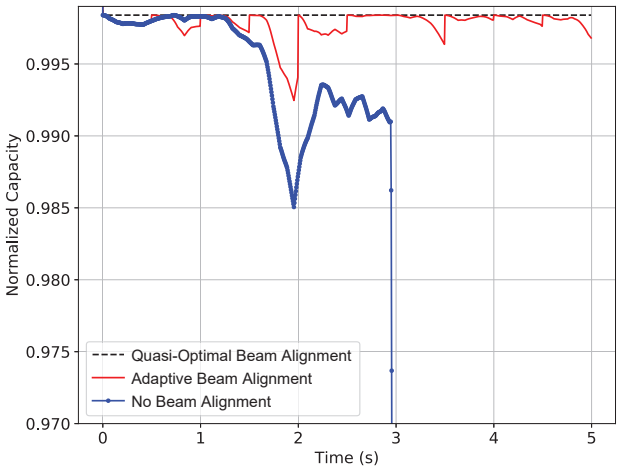

Fig. 8: Normalized link capacity with micro-scale mobility for transmitter, small-scale mobility for receiver, and directivity angle of 5°.

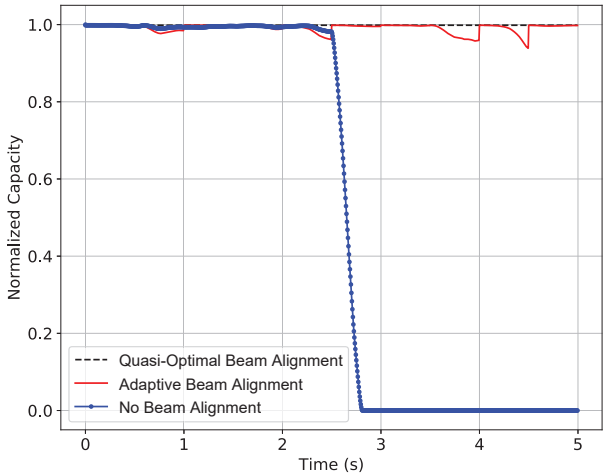

Fig. 9: Normalized link capacity with small-scale mobility and directivity angle of 5°.

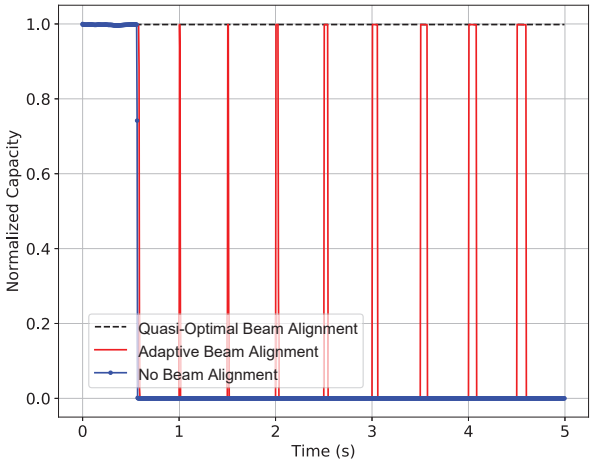

Fig. 10: Normalized link capacity with large-scale mobility and directivity angle of 5°.

frequent than in Scenario 1. This feature can be exploited in the design of adaptive communication protocols to achieve the optimal time allocation between beam alignment and data transmission.

The results of large-scale mobility are plotted in Fig. 7. The directivity angle is the same as in Figs. 5 and 6. In the tested instance, if no beam alignment is adopted the drones experience a constant outage after less than one second because of the significant misalignment between the transmit and receive antennas. Intermittent outages occur in more than 50% of the time even with adaptive beam alignment of latency 0.5s. Therefore, frequent low-latency beam alignments are required to mitigate the negative effects of the mobility uncertainties of the drones in this scenario.

Figures 8, 9 and 10 plot the normalized capacity in the case of directivity angle equal to 5°. Unsurprisingly, the drones are more likely to experience outages with narrower beamwidth. For example, in Fig. 10 the outage occurs in around 0.125s after every time of the beamalignments, which is around 0.25s with directivity angle of 10° in Fig. 7. Since narrow beamwidth is essential for mmWave/THz communications to achieve higher signal-to-noise ratio (SNR) with extended communication distance, it is worth investigating dynamic beamwidth adaptation protocols to achieve a good trade-off between low outage probability and high link capacity.

VI. Conclusions

In this paper we have studied the effects of mobility uncertainties on mmWave/THz-band communications between flying drones. The mobility uncertainties of the flying drones were characterized based on a series of field measurements. The link capacity of the mmWave/Thz links has been analyzed in the presence of micro-, small- and large-scale mobility uncertainties. It is found that the negative effects of micro-scale mobility on the link capacity is negligible and therefore not needed to be considered in the protocol design. With small- and large-scale mobility, significant performance degradation and link outages have been observed. A future research direction is to design adaptive transmission protocols by jointly controlling the beam alignment frequency and the directivity angle for wireless drone networking in the mmWave/THz bands in the presence of small- and large-scale mobility uncertainties as well as in different weather conditions.

Acknowledgement

The authors are thankful to the anonymous referees for their helpful insights, which improved the quality of the paper.

References

[1] I. F. Akyildiz, C. Han, and S. Nie, "Combating the Distance Problem in the Millimeter Wave and Terahertz Frequency Bands," *IEEE Communications Magazine*, vol. 56, no. 6, pp. 102–108, June 2018.

[2] M. Xiao, S. Mumtaz, Y. Huang, L. Dai, Y. Li, M. Matthaiou, G. K. Karagiannidis, E. Björnson, K. Yang, C.-L. I, and A. Ghosh, "Millimeter Wave Communications for Future Mobile Networks," *IEEE Journal on Selected Areas in Communications*, vol. 35, no. 9, pp. 1909 – 1911, Sept. 2017.

[3] A. S. Cacciapuoti, K. Sankhe, M. Caleffi, and K. R. Chowdhury, "Beyond 5G: THz-Based Medium Access Protocol for Mobile Heterogeneous Networks," *IEEE Communications Magazine*, vol. 56, no. 6, pp. 110–115, June 2018.

[4] E. Başтuğ, M. Bennis, M. Médard, and M. Debbah, "Toward Interconnected Virtual Reality: Opportunities, Challenges, and Enablers," *IEEE Communications Magazine*, vol. 55, no. 6, pp. 110–117, June 2017.

[5] Q. Xia and J. M. Jornet, "Leveraging Antenna Side-Lobe Information for Expedited Neighbor Discovery in Directional Terahertz Communication Networks," in *Proc. of IEEE VTC*, Porto, Portugal, July 2018.

[6] I. Bor-Yaliniz and H. Yanikomeroglu, "The New Frontier in RAN Heterogeneity: Multi-Tier Drone-Cells," *IEEE Communications Magazine*, vol. 54, no. 11, pp. 48–55, Nov. 2016.

[7] H. Wang, G. Ding, F. Gao, J. Chen, J. Wang, and L. Wang, "Power Control in UAV-Supported Ultra Dense Networks: Communications, Caching, and Energy Transfer," *IEEE Communications Magazine*, vol. 56, no. 6, pp. 28–34, June 2018.

[8] Y. Zeng, R. Zhang, and T. J. Lim, "Wireless Communications with Unmanned Aerial Vehicles: Opportunities and Challenges," *IEEE Communications Magazine*, vol. May, no. 54, p. 5, 36-42 2016.

[9] Z. Guan, N. Cen, T. Melodia, and S. Pudlewski, "Self-Organizing Flying Drones with Massive MIMO Networking," in *Proc. of Mediterranean Ad Hoc Networking Workshop (Med-Hoc-Net)*, Capri, Italy, June 2018.

[10] L. Zhang, Z. Guan, and T. Melodia, "United Against the Enemy: Anti-Jamming Based on Cross-Layer Cooperation in Wireless Networks," *IEEE Transactions on Wireless Communications*, vol. 15, no. 8, pp. 5733–5747, Aug 2016.

[11] N. Cheng, W. Xu, W. Shi, Y. Zhou, N. Lu, H. Zhou, and X. S. Shen, "Air-Ground Integrated Mobile Edge Networks: Architecture, Challenges and Opportunities," *IEEE Communications Magazine*, vol. 56, no. 8, pp. 26–32, August 2018.

[12] M. K. Haider and E. W. Knightly, "Mobility Resilience and Overhead Constrained Adaptation in Directional 60 GHz WLANs: Protocol Design and System Implementation," in *Proc. of MobiHoc*, Paderborn, Germany, July 2016.

[13] H. Hassanieh, O. Abari, M. Rodriguez, M. Abdelghany, D. Katabi, and P. Indyk, "Fast MillimeterWave Beam Alignment," in *Proc. of SIGCOMM*, Budapest, Hungary, August 2018.

[14] C. Zhang, K. Ota, J. Jia, and M. Dong, "Breaking the Blockage for Big Data Transmission: Gigabit Road Communication in Autonomous Vehicles," *IEEE Communications Magazine*, vol. 56, no. 6, pp. 152–157, June 2018.

[15] V. Petrov, J. Kokkoniemi, D. Moltchanov, J. Lehtomäki, M. Juntti, and Y. Koucheryavy, "The Impact of Interference From the Side Lanes on mmWave/THz Band V2V Communication Systems With Directional Antennas," *IEEE Trans. on Vehicular Technology*, vol. 67, no. 6, pp. 5028–5041, June 2018.

[16] Z. Li, L. Guan, C. Li, and A. Radwan, "A Secure Intelligent Spectrum Control Strategy for Future THz Mobile Heterogeneous Networks," *IEEE Communications Magazine*, vol. 56, no. 6, pp. 116–123, June 2018.

[17] Z. Xiao, P. Xia, and X.-G. Xia, "Enabling UAV Cellular with Millimeter-Wave Communication: Potentials and Approaches," *IEEE Communications Magazine*, vol. 54, no. 5, pp. 66–73, May 2016.

[18] S. Mumtaz, J. M. Jornet, J. Aulin, W. H. Gerstacker, X. Dong, and B. Ai, "Terahertz Communication for Vehicular Networks," *IEEE Trans. on Vehicular Technology*, vol. 66, no. 7, pp. 5617–5624, July 2017.

[19] V. Petrov, D. Moltchanov, Y. Koucheryavy, and J. M. Jornet, "The Effect of Small-Scale Mobility on Terahertz Band Communications," in *Proc. ACM/IEEE International Conference on Nanoscale Computing and Communication (NanoCom)*, Reykjavik, Iceland, Sept. 2018.

[20] R. Kovalchukov, D. Moltchanov, A. Samuylov, A. Ometov, S. Andreev, Y. Koucheryavy, and K. Samouylov, "Analyzing Effects of Directionality and Random Heights in Drone-based mmWave Communication," *IEEE Transactions on Vehicular Technology*, vol. 67, no. 10, pp. 10 064–10 069, Oct. 2018.

[21] J. M. Jornet and I. F. Akyildiz, "Channel Modeling and Capacity Analysis of Electromagnetic Wireless Nanonetworks in The Terahertz Band," *IEEE Transactions on Wireless Communications*, vol. 10, no. 10, pp. 3211–3221, Oct. 2011.

[22] V. Petrov, M. Komarov, D. Moltchanov, J. M. Jornet, and Y. Koucheryavy, "Interference Analysis of EHF/THF Communications Systems with Blocking and Directional Antennas," in *Proc. of IEEE GLOBECOM*, Singapore, Dec. 2016.

[23] J. M. Jornet and I. F. Akyildiz, "Femtosecond-long Pulse-based Modulation for Terahertz Band Communication in Nanonetworks," *IEEE Trans. on Communications*, vol. 62, no. 5, pp. 1742–1754, May 2014.